Skeletal Radiology (2022) 51:451–475
https://doi.org/10.1007/s00256-021-03842-4

REVIEW ARTICLE

Periarticular calcifications

Y. Y. Yan[1,2] · Y. N. Bin Dous[1] · H. A. Ouellette[1] · P. L. Munk[1] · N. Murray[1] · P. I. Mallinson[1] · M. A. Sheikh[1]

Received: 9 April 2021 / Revised: 12 June 2021 / Accepted: 13 June 2021 / Published online: 21 June 2021

Abstract
Periarticular calcification and ossification is a frequent finding on imaging and may sometimes pose a diagnostic challenge. The differential diagnoses for this radiological finding are wide and can be classified into broad groups such as idiopathic, developmental, trauma, burns, infection, tumor, connective tissue disease, crystalline, metabolic, vascular, and foreign bodies. With careful consideration of the clinical and imaging findings as well as awareness of mimickers of periarticular mineralization, the list of differential diagnoses can be narrowed down. This article aims to review the clinical-radiologic findings of periarticular calcified or ossified lesions with relevant imaging illustrations.

Keywords Periarticular mineralization · Calcified malignancy · Calcinosis · Synovial sarcoma · Ossification

Introduction

Periarticular calcifications and ossifications are commonly encountered in a variety of imaging modalities either incidentally or in relation to the clinical question. It is important to recognize these calcifications' clinical relevance and whether evaluation with further imaging is required.

The periarticular space consists of different tissue types and structures. It can be broadly categorized into intra-articular and extra-articular components. The joint capsule demarcates the boundary for intra-articular structures and may contain fibrocartilage, hyaline cartilage, synovium, and synovial fluid. Extra-articular structures in the joints' vicinity include the bursae, ligaments, muscles, tendons, tenosynovium, vascular, nervous, skin, subcutaneous, and fascial tissues [1]. Each of the structures may be affected by different pathological disorders.

A general guide to assist the radiologist in distinguishing the various causes of periarticular calcifications is as follows. Differentiating between calcifications and ossification should be carried out first, by observing that calcifications usually appear as mineralized densities while mature ossification demonstrates an outer cortex and internal trabeculae [2]. This is followed by systematically reviewing different etiologies to generate a list of differential diagnoses when assessing periarticular mineralization (Table 1). A list of conditions leading to periarticular calcifications can be further subdivided into multi-regional and single region involvement to assist in diagnosing (Table 1). Etiologies to consider for solitary calcifications include idiopathic tumoral calcinosis, infection, crystalline, foreign body, tumor, and vascular conditions, while etiologies in multi-regional calcifications include metabolic, connective tissue disease, infection, crystalline, and vascular conditions. Traumatic causes such as myositis ossificans and tumoral causes such as synovial chondromatosis and soft tissue chondroma can exhibit both calcification and ossification. Ossifications tend to be post-traumatic, while calcifications, although having variable etiologies, are associated with crystalline causes. It is also important to be cognizant of mimickers of periarticular mineralization and ossification — conditions that look very similar to these densities (for example, metallosis) or lesions that are strictly not periarticular and are contiguous with bone or metaphyseal in location (Table 1). Etiologies of mimickers consist of developmental, inflammatory arthropathy, tumor, trauma, and iatrogenic causes.

Mineralization can be broadly categorized into dystrophic and metabolic causes. Dystrophic calcifications, comprising most calcifications, occur in necrotic or damaged tissue with normal serum levels of calcium and may progress to

✉ Y. Y. Yan
yanyetyen@gmail.com

[1] Department of Radiology, Musculoskeletal Section, Vancouver General Hospital, University of British Columbia, Vancouver, BC, Canada

[2] Department of Radiology, Changi General Hospital, 2 Simei Street 3, Singapore 529889, Singapore

Table 1 Main differential diagnoses of periarticular calcification and ossification. Labeled alphanumeric characters refer to corresponding sections in the manuscript

Calcification		Ossification	Calcification and Ossification	Mimics
Solitary	Multi-regional			
Calcinosis (1) • Idiopathic tumoral calcinosis (a)	Calcinosis (1) • Metabolic (b) - End-stage renal disease • Connective tissue disease (c) - Scleroderma	Trauma (4) • Avulsion fracture (c)	Trauma (4) • Myositis ossificans (a)	Trauma/stress (10) • Enthesophyte (a) • BPOP (b) • Florid reactive periostitis (c)
Infection (2)	Infection (2) (may have a specific configuration)	Burns (5)	Tumor (7) • Synovial chondromatosis (b) • Soft tissue chondroma (c)	Tumor (11) • Surface bone tumors/sarcoma (a) • Periosteal chondroma (b)
Vascular (3) • Vascular malformation (a)	Vascular (3) • Atherosclerotic plaques (a) • Monckeberg's medial sclerosis (b) • Vascular malformations (c)	Developmental (9) • Accessory ossicles/sesamoids (a)		Developmental (12) • Osteochondroma (a)
Crystalline (6) • HADD (b) (more common)	Crystalline (6) • Gout (a) • HADD (b) (less common) • CPPD (c)			Inflammatory arthropathy (13) • Psoriatic related bony proliferation and periostitis (a)
Tumor (7) • Synovial sarcoma (a)				Iatrogenic (14) • Metallosis (a)
Foreign body (8)				

Abbreviations: *HADD* calcium hydroxyapatite deposition disease, *CPPD* calcium pyrophosphate deposition disease, *BPOP* bizarre parosteal osteochondromatous proliferation

ossification. Metabolic (sometimes referred to as metastatic) calcifications are generally diffuse and are associated with abnormal serum levels of calcium, phosphate, and other ions.

Calcifications are mineralized densities with an attenuation coefficient between that of soft tissue and bone, while mature bone is more structured with corticated and trabecular components [2]. Although conventional radiography is usually the first imaging modality to depict mineralization, CT is more sensitive. On computed tomography (CT), calcifications have Hounsfield unit (HU) values of usually between 100 and 400, while bones show higher HU values (700 HU for trabecular bone and exceeding 1500 HU for cortical bone) [2]. Dual-energy CT (DECT) has the additional benefit of utilizing spectral properties to discern the chemical composition of these calcifications [3, 4]. Although CT is the current reference standard for the detection of calcifications, it is associated with ionizing radiation. On the contrary, magnetic resonance imaging (MRI) does not utilize ionizing radiation but is insensitive to calcifications. Interpretation of MRI should be supplemented with radiograph when the presence of mineralization is an important diagnostic clue. When calcifications are detected on MRI, they usually appear signal hypointense but can show variable signal intensities on conventional spin echo T1- or T2-weighted images. However, gradient echo sequences and susceptibility-weighted imaging can be utilized to improve the identification of calcifications. When compared to conventional CT, the pooled sensitivities of susceptibility-weighted imaging and standard MRI are 86.5% and 36.7%, respectively, while the pooled specificities of susceptibility-weighted imaging and standard MRI are comparable at 90.8% and 94.2%, respectively [5]. In addition, MRI is shown to yield lower volumes than CT in the measurement of calcifications [6]. While radiography only permits 2-dimensional assessment of calcifications, the radiographic area has been shown to highly correlate with CT and MRI volumes

and radiographs may provide comparable information to CT or MRI on the volume of calcifications [6]. Although ultrasound (US) is more sensitive than radiography in detecting calcifications, it is operator dependent and the presence of acoustic shadowing precludes a thorough examination. Mature ossification is recognized by the presence of cortex, internal trabeculae, and fatty marrow on CT and MRI. It may be challenging distinguishing immature bone from calcifications.

Calcinosis

Idiopathic

Idiopathic tumoral calcinosis, a rare inherited disorder of dysregulated phosphate metabolism, is characterized by large masses of intramuscular and/or subcutaneous calcifications in the juxta-articular soft tissues and extensor aspect of the extremities (bursal distribution). Phosphate levels are increased in the familial form and normal in the sporadic form. The disease is typically seen in patients of African descent and individuals in the first and second decades of their life. Most of these patients are asymptomatic, although they can show decreased range of motion secondary to mass effect. Lesions are typically not painful unless there is compression of adjacent nerves [7]. These lesions can grow slowly over time [8]. These lesions commonly occur adjacent to large joints such as the hips and shoulders and to a lesser extent around the elbows, knees, and feet. Radiographically, they are lobulated masses ranging in size from 1 to 20 cm^2. They are composed of radiodense calcified material with intervening radiolucent bands of fibrous septa (Fig. 1). The radiodense regions may be homogeneously dense or occasionally show fluid–fluid levels. Bony erosion is usually absent. On CT, they are lobulated cystic calcifications, which often communicate with the bursa (Fig. 1). On MRI, they are heterogeneously T1 hypointense with low signal intensity and diffusely T2 hypointense or a bright nodular pattern with alternating areas of high T2 signal intensity (Fig. 1).

Metastatic (metabolic)

Metastatic (metabolic) calcifications are generalized calcifications associated with abnormal calcium and/or phosphate levels [2, 7]. End-stage renal disease, the most common cause of metastatic calcifications, is a major cause of massive periarticular calcifications. This metabolic disorder secondary to renal dysfunction shows a correlation with the duration of the underlying renal disease and may occur in the absence of hyperparathyroidism [1, 7, 9]. Metastatic calcifications consist of periarticular lobulated calcified masses that are usually multicystic and contain fluid–fluid levels (Fig. 2). These periarticular masses may resemble idiopathic tumoral calcinosis except for the presence of bone erosion and destruction. Associated vascular calcifications, chondrocalcinosis, bone resorption, osteopenia or osteosclerosis, and tendon pathologies may occur. Other causes of metastatic calcifications include primary hyperparathyroidism, milk-alkali syndrome, and hypervitaminosis D.

Connective tissue disease

Calcinosis circumscripta is usually associated with scleroderma [10]. The calcinosis of scleroderma mostly involves the subcutaneous tissue and consists of calcium apatite crystals and is not associated with any calcium metabolism dysregulation. Deposits are present in the hands (in over half of afflicted individuals) and feet as well as areas of the extremities such as the elbow that frequently undergo friction or mild trauma [8]. The calcinosis of scleroderma often shows a cobblestone appearance, which may appear similar to that of end-stage renal disease or tumoral calcinosis but are less extensive without septa or fluid–fluid levels (Fig. 3). Involvement of the hands, a location rarely afflicted by other causes of calcification, combined with the presence of acro-osteolysis and distal phalangeal soft tissue atrophy, is a characteristic of scleroderma. Mixed connective tissue disease and, infrequently, lupus erythematosus may also occasionally show calcinosis [2].

Infection

Chronic infection can lead to dystrophic calcifications. Musculoskeletal tuberculosis involving bursa and tendon sheath can cause a periarticular pattern of calcifications arising from caseating material. Musculoskeletal tuberculosis most commonly affects the trochanteric, subacromial, subgluteal, and radioulnar wrist bursae as well as the flexor tendon sheaths of hands and feet and peroneal tendon sheaths [11]. Some calcifications with a characteristic appearance such as small “cigar-shaped” intramuscular and subcutaneous calcifications are seen in cysticercosis (Fig. 4). Other infections giving rise to a typical configuration of calcifications include trichinosis, dracunculiasis, and peripheral nerve calcification in leprosy.

Fig. 1 A 57-year-old man with tumoral calcinosis. **a** Right hip anteroposterior radiograph shows a well-defined calcified mass projected over the inferior aspect of the right hip. **b** Axial CT shows a lobulated intramuscular calcified mass extending from the trochanteric bursa into the ischiofemoral space (arrowhead) and causing secondary ischiofemoral impingement and sciatic nerve indentation without any bony erosion. **c, d** Axial T2-weighted fat suppression image (**c**) and postgadolinium T1-weighted fat suppression image (**d**) show this lesion to have a heterogeneous appearance and no altered signal within the sciatic nerve (arrow)

Vascular

Venous calcifications, a reflection of chronic venous insufficiency, are generally seen in the superficial venous system and therefore mostly limited to the subcutaneous compartment. Their development occurs in the presence of long-standing varicosities and/or thrombus formation. These factors result in venous stasis, leading to calcium deposition along the venous intimal layer [8]. Venous calcifications are more commonly seen in women and almost exclusively affect the lower limbs except in upper limb venous stasis from causes such as prior trauma, surgery, or other conditions that alter normal venous drainage. Phleboliths, representing venous thrombi, are well-defined calcific foci with denser rims and central lucencies.

The calcium deposits associated with arteries can be classified into two groups, atherosclerotic plaques and Monckeberg's medial sclerosis. Dystrophic atherosclerotic plaque calcifications typically involve the

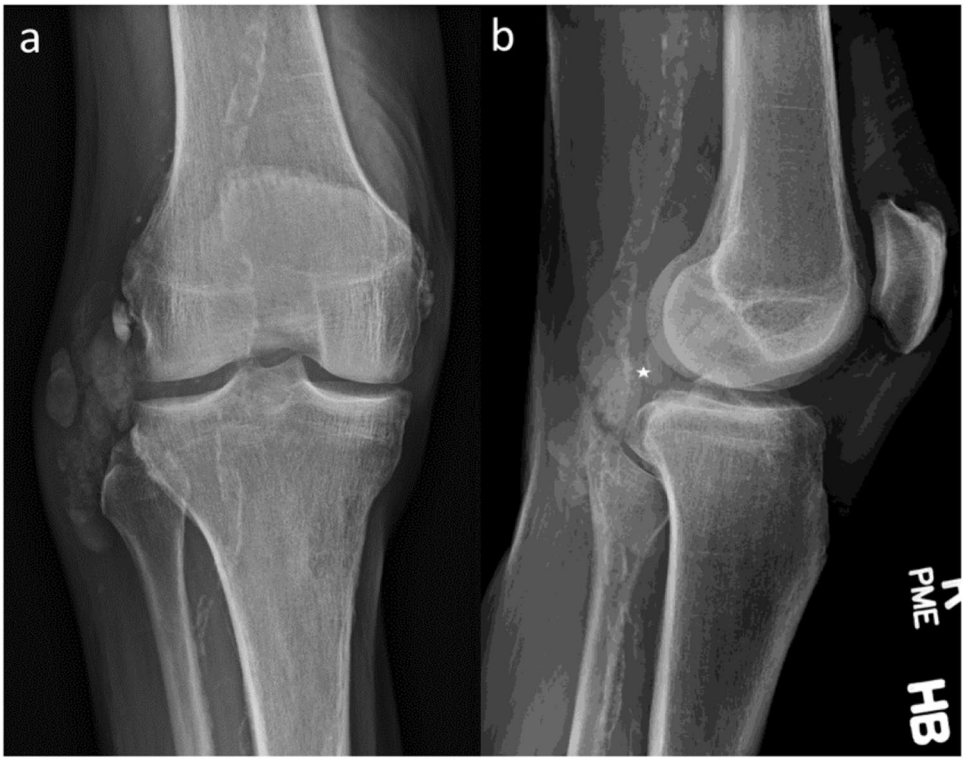

Fig. 2 A 83-year-old man with end-stage renal disease-related calcinosis. **a, b** Right knee anteroposterior radiograph (**a**) and lateral radiograph (**b**) show lobulated calcified lesions projected posterolateral to the right lateral femorotibial joint (star) and over the expected locations of the proximal collateral ligaments of the knee. Associated chondrocalcinosis and prominent uniform thin linear and continuous calcifications of Monckeberg's medial sclerosis involving the popliteal artery and its branches

large- and medium-sized arteries, resulting in narrowing the vessel lumen, affecting the intima, and appearing as patchy, irregular, plaque-like, or tubular densities of variable shape and size. On the contrary, metabolic Monckeberg calcifications characterized by a disorder in phosphate metabolism [12] are predominantly seen in type 2 diabetes mellitus and chronic renal failure, involve the media, and predominate in the small arteries of the distal extremities, particularly the feet. The calcifications of Monckeberg's medial sclerosis are more often uniform linear, thin, and continuous as compared to that of peripheral vascular disease (Fig. 2).

Fig. 3 A 84-year-old woman with scleroderma. Bilateral hands anteroposterior radiograph shows large conglomerate subcutaneous soft tissue calcifications projected around the distal ulna and dorso-ulnar aspects of both carpi, left more pronounced than right. Mild to moderate amounts of similar soft tissue calcifications are scattered over the right radiocarpal, bilateral first carpometacarpal, almost all metacarpophalangeal, and interphalangeal joints, more prominent in bilateral second to third distal interphalangeal joints. Associated bilateral scattered erosions are also evident, for example, involving the right fourth and fifth and left third and fifth proximal interphalangeal joints

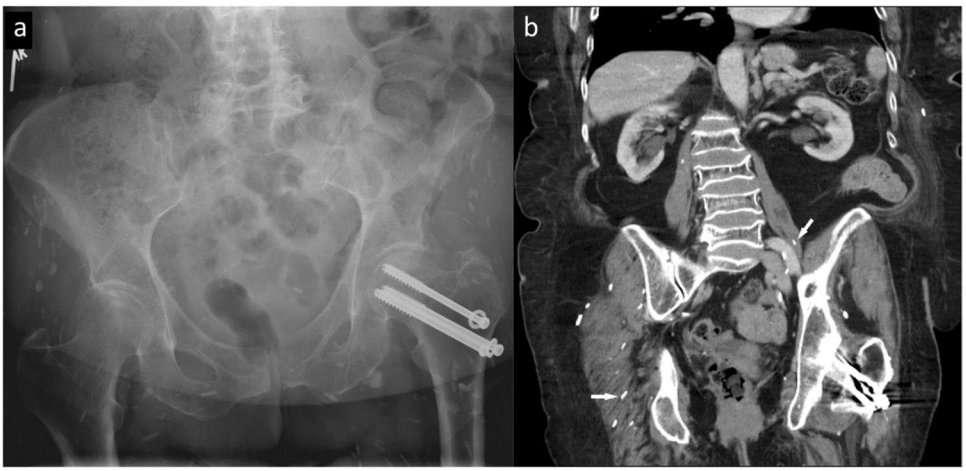

Fig. 4 A 84-year-old woman with cysticercosis. **a** Pelvis anteroposterior radiograph shows innumerable elongated calcific densities of a "cigar-shaped" configuration scattered over the soft tissues of bilateral pelvis. **b** Coronal CT shows these calcific densities predominantly oriented longitudinally along the muscle fibers of bilateral psoas and pelvic girdle muscles (arrows). Incidental multiple lumbar compression fractures and screw fixation of old neck of left femur fracture

According to the International Society for the Study of Vascular Anomalies (ISSVA), vascular malformations and tumors are categorized into a complex classification [13]. A comprehensive discussion of the various clinical-radiological findings of each entity is beyond the scope of this article. Symptoms may include pain, impaired mobility, and skeletal deformity. Venous malformations can show occasional phleboliths and, less frequently, with adjacent skeletal anomalies. On the contrary, high-flow vascular lesions tend to produce more "tram-track" calcifications seen in arteries and not phleboliths. On US, venous malformations have highly variable appearances (ill defined or well defined), usually showing heterogeneous echogenicity with multiple cystic spaces, and may or may not show internal vascularity. CT can demonstrate phleboliths as well as possible fatty soft tissue components. MRI depicts best the extent of disease involvement. Venous malformations can be infiltrative and extend across multiple tissue planes (fat, muscle, tendon, bone) [14]. Venous malformations appear as septated lobulated, often highly infiltrative, T2 hyperintense masses with frequent fluid–fluid levels, no-flow voids, and slow gradual enhancement on delayed images [14] (Fig. 5). Fat is commonly interspersed between stromal elements and fluid pockets and perilesional edema may be present [14].

Trauma

Myositis ossificans

Myositis ossificans is a benign intramuscular bone proliferation [15]. Heterotopic ossification is neither specific to muscle nor involves prominent inflammation after its early stages [16]. Young active males are most affected, with the classic clinical history being pain, swelling, and joint stiffness following blunt soft tissue trauma [17]. However, clinical presentation is variable and depends on disease stage [17]. Myositis ossificans can also be secondary to burns, immobilization, or neurologic dysfunction although it most commonly occurs after trauma. Myositis ossificans undergoes 3 stages characterized by varying degrees of calcification and/or ossification: an early (< 4 weeks), intermediate (4–8 weeks), and mature stage (> 8 weeks) [17]. In the early stage, calcifications are usually not apparent. In the intermediate stage, amorphous calcifications appear. These calcifications produce a densely calcified peripheral rim with a lucent center, typically by the end of the intermediate stage. The mature stage is characterized by a peripheral rim of calcification resembling cortical bone. Mature lesions may show diffuse ossification, usually run in parallel with the long axis of the muscle, and often have a radiolucent cleft that separates it from adjacent bone [17]. The temporal evolution of the appearance and maturation of the calcification in myositis ossificans is related to the patient's age and these reference time frames serve as a guide due to influence by age [18].

The classical temporal sequential changes in radiography and CT is diagnostic for myositis ossificans. Myositis ossificans has a varying appearance at MRI, depending on disease stage [17]. In the early stage, lesions may be poorly defined and show enhancement, hemorrhage, fluid–fluid levels, and surrounding soft tissue edema, simulating an aggressive tumor, or it may show a thick enhancing rim mimicking an abscess [15, 17]. Intermediate lesions exhibit a predominantly cellular core of active fibroblasts before exhibiting more well-defined margins and faint rim calcifications (Fig. 6). Early calcifications can be difficult to detect on MRI and are best

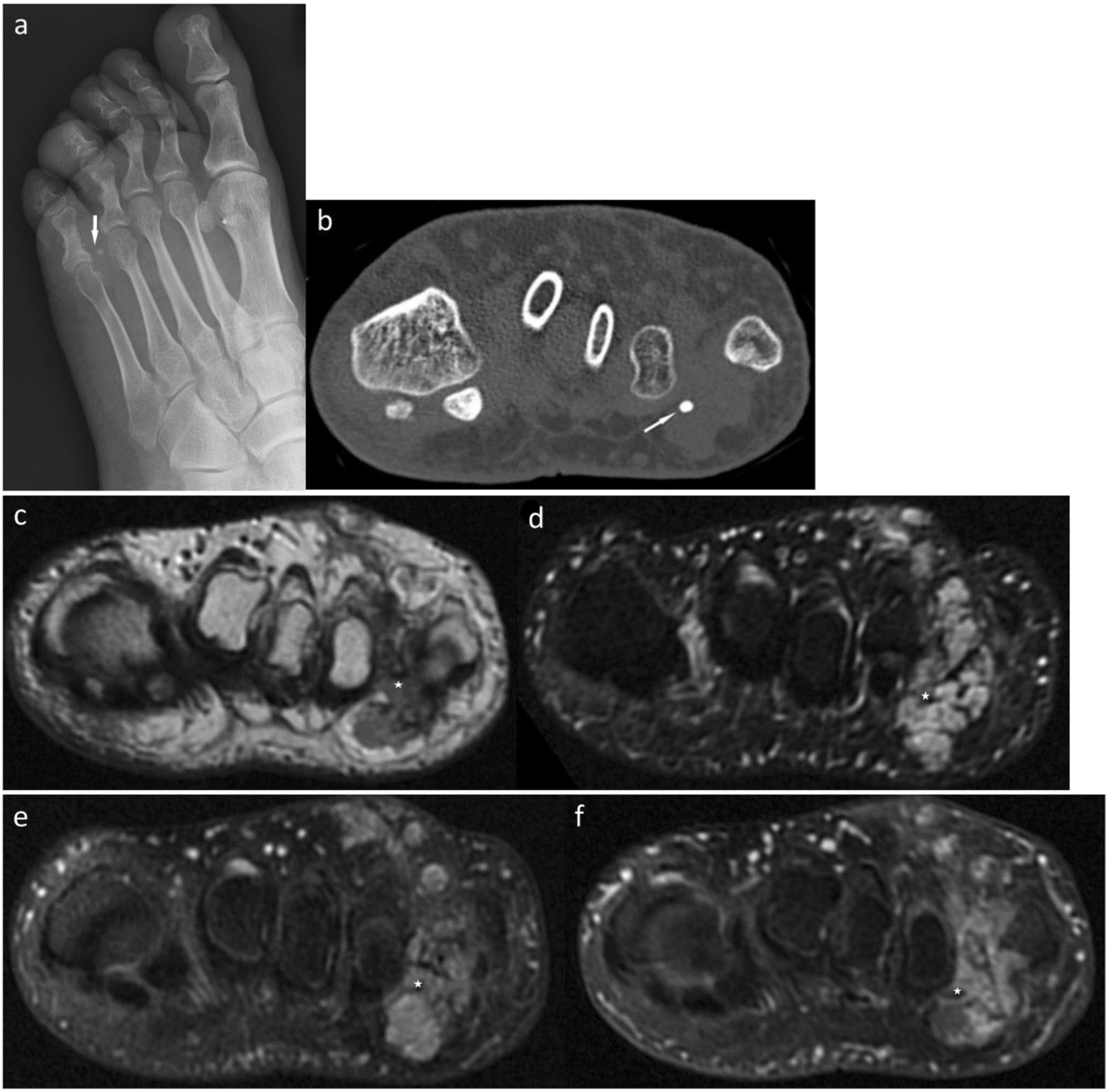

Fig. 5 A 47-year-old man with slow flow vascular malformation. **a** Left foot oblique radiograph shows a calcific focus compatible with a phlebolith projected over the 4th web space. **b** Coronal CT confirms a subcutaneous lobulated lesion with an internal phebolith in the 4th web space without any bony erosion. **c, d** Coronal T1-weighted image (**c**) and coronal short tau inversion recovery (STIR) image (**d**) shows a lobulated STIR hyperintense lesion (star) involving the lateral aspect of the 4th digit extending proximally from the level of the phalanges to the metatarsophalangeal joint. No underlying bony involvement. The phleboliths seen on the previous radiographs are not easily appreciable on the MRI. **e, f** Coronal pre- (**e**) and postgadolinium T1-weighted fat suppression image (**f**) shows this lesion to be mildly enhancing (star)

demonstrated on CT [19]. Extensive perilesional muscle edema on MRI of more than double the size of the central lesion is highly specific, but not pathognomonic for myositis ossificans in the early/intermediate stage, and can be utilized in the differentiation from malignant intramuscular soft tissue lesions [20]. Mature lesions demonstrate the distinctive zonal organization of myositis ossificans, with a peripheral ring of mature ossification at its margins surrounding a central cellular core and resolution of surrounding edema [17, 18]. With increasing

Fig. 6 A 31-year-old woman with intermediate stage myositis ossificans. **a** Right lateral hip radiograph demonstrates a faintly calcified soft tissue lesion anterior to the right femur trochanter region. **b** Targeted longitudinal ultrasound over the right lower hip shows an intramuscular lesion with an echogenic rim in the vastus intermedius exhibiting posterior acoustic shadowing (arrow). **c** Axial CT performed on the same day as ultrasound shows a vastus intermedius intramuscular lesion with a peripheral dense rim of calcification (zoning phenomenon). **d, e, f, g** Axial T1-weighted image (**d**), T2-weighted with fat suppression image (**e**), pre- (**f**) and postgadolinium T1-weighted fat suppression image (**g**) performed 2 weeks before the CT and radiograph show a heterogeneously enhancing intramuscular mass (dotted arrow) within the right proximal quadriceps muscle predominantly involving the vastus intermedius muscle at the subtrochanteric level with marked peri-lesional edema (solid arrow). No lesional calcification was seen then

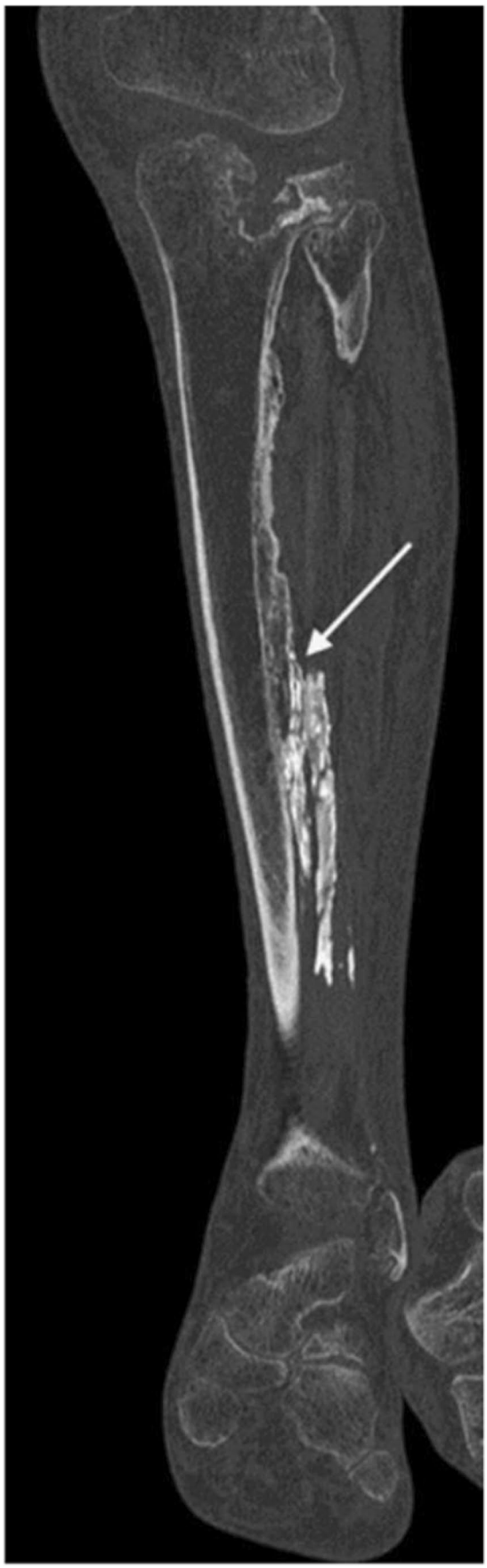

Fig. 7 A 59-year-old man with calcific myonecrosis. Coronal CT ▶ depicts extensive peripheral sheet like calcified lesion (arrow) in the anterior compartment muscles of the left calf with overlying wound. Background of old left proximal tibia fracture with previous internal fixation changes

maturation, the cellular central core changes into mature fat-containing marrow. The intense tracer avidity seen in bone scintigraphy and fluorodeoxyglucose (FDG) positron emission tomography (PET) in early and intermediate stages progressively decreases as maturation occurs [17, 21]. On US, acoustic shadowing from the osseous rim of the lesion precludes a comprehensive evaluation of the lesion. Close imaging surveillance or biopsy should be considered whenever the diagnosis of myositis ossificans is in doubt and referral to a Sarcoma center should be performed. However, early biopsy is not recommended because it can be challenging differentiating myositis ossificans from sarcoma [22].

Calcific myonecrosis

Calcific myonecrosis is a rare condition characterized by a painful slowly growing mass. The lower leg's anterior compartment muscles are the most common site, although it can occur in other muscles of the lower limb and forearm [23] (Fig. 7). The mass in calcific myonecrosis demonstrates a liquefied center and peripheral often sheet like calcifications and is often mistaken for myositis ossificans. However, unlike myositis ossificans, calcific myonecrosis involves the entire muscle or compartment and presents as a chronic expanding mass [23]. Adjacent healed fractures are often seen.

Avulsion fracture

Avulsion fracture occurs when the origin of ligament or tendon is forcefully separated from bone. There is underlying bony disruption, although the tendon or ligament usually remains intact. Avulsion fractures are common in participants of organized sports, particularly skeletally immature athletes due to the inherent weakness of their apophyses. Adults with bones compromised by osteoporosis or tumor are also vulnerable to such injuries.

In radiography, avulsion fractures are often subtle and the avulsed bone fragment is typically displaced in the direction of the soft tissue structure it is attached to. Acutely, a partially corticated bony fragment with a donor site and associated soft tissue swelling may be seen. This contrasts with the regular smoothly corticated appearance of sesamoids/accessory ossicles that are seen in characteristic locations [24]. Subacute avulsion

fractures may show mixed lytic and sclerotic areas owing to different stages of bone healing. In chronic avulsion fractures, radiographs display bony sclerosis and hypertrophy at the avulsion site as well as calcification and thickening at the avulsed end of the tendon. CT and MRI can be used to assess the extent of the injury and injury to the musculotendinous structures. On MRI, small avulsion fractures can be easily missed, as the avulsed osseous fragment is often poorly seen, and bone marrow edema may be absent at the avulsion site [25]. An accurate diagnosis requires awareness of usual radiographic patterns and proficiency in musculotendinous anatomy. Chronic avulsion fractures can be diagnostically challenging and mimic osteomyelitis and

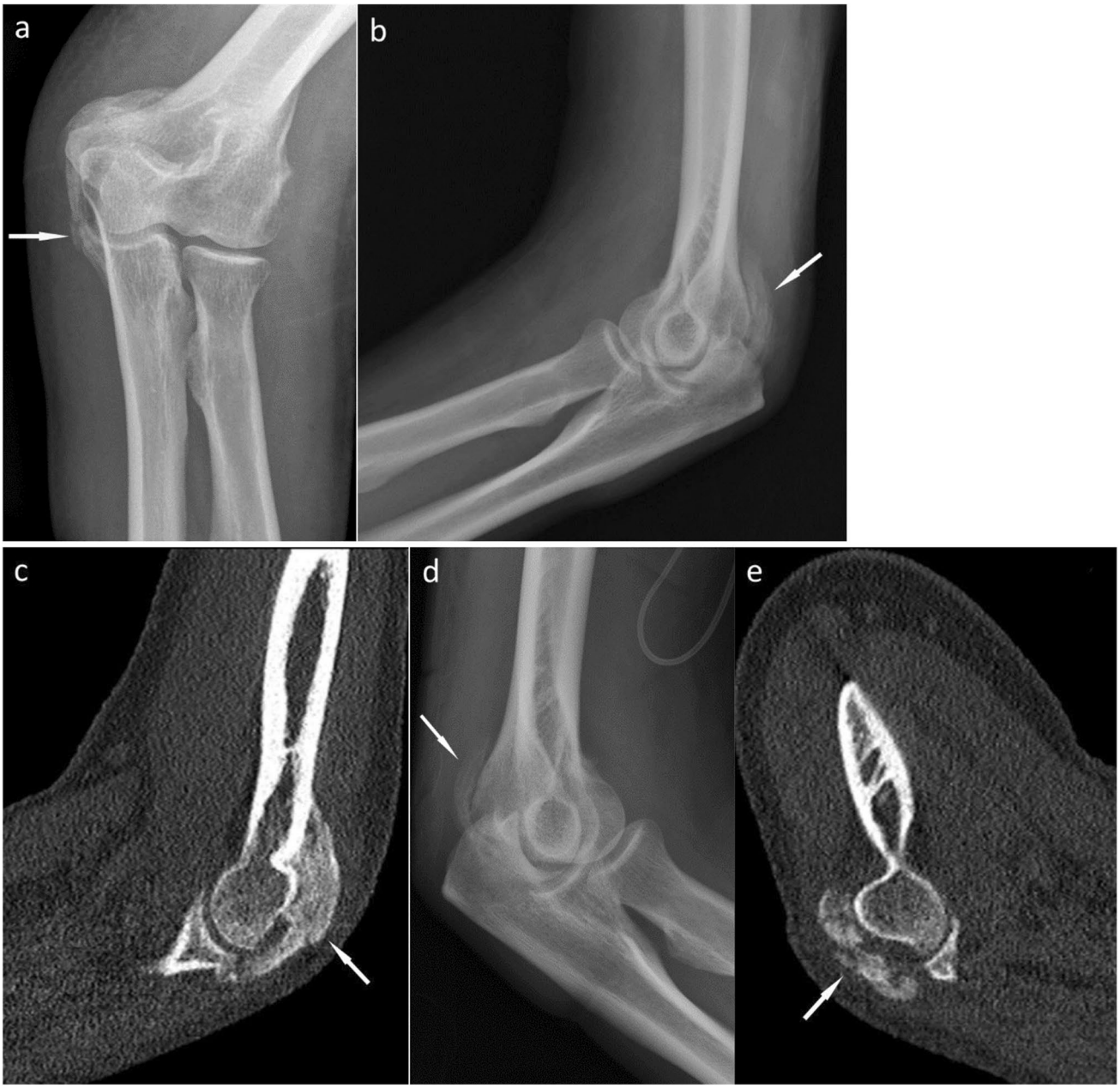

Fig. 8 A 55-year-old man with heterotopic ossification. 2 months after suffering a 39.5% total body surface area burns injury, he presented with restricted range of motion of bilateral elbows and subsequently underwent removal of heterotopic ossification and osteocaspular arthroplasty of bilateral elbows. **a, b, c** Left elbow anteroposterior radiograph (**a**), left elbow lateral radiograph (**b**) and sagittal CT left elbow (**c**) show heterotopic ossification partially fusing the posterolateral ulnotrochlear articulation. **d, e** Right elbow lateral radiograph (**d**) and sagittal CT right elbow (**e**) show heterotopic ossification partially fusing the posterior ulnotrochlear articulation

bone tumors [25]. The majority of avulsion fractures are managed conservatively.

Burns

Heterotopic ossification after burns injury is a rare but well-known complication that can cause significant morbidity, especially around the elbow joint [26]. These ossifications can cause limited range of motion and function, severe pain, and nerve entrapment [26]. Clinical signs of heterotopic ossification precede radiological confirmation by a mean of at least 5 days to several weeks [27]. Heterotopic ossification generally is not detected on radiography until 4 to 8 weeks after the initial symptoms [28] (Fig. 8).

Crystalline

Gout

Gout is a crystal-induced arthropathy resulting from monosodium urate (MSU) crystals deposited within joints and surrounding soft tissues. Risk factors for gout include dietary, obesity, hypertension, renal impairment, and diuretic use [29]. In radiography and CT, gouty tophi may manifest as hyperdense soft tissue swelling and presence of dense calcifications is a late finding [30]. Radiography is economical and effective in identifying advanced chronic gouty arthritis [31]. CT is the gold standard for imaging any associated bone erosions. Tophi have a characteristic density of around 160 HU [32]. DECT can be used to detect MSU

Fig. 9 A 70-year-old man with chronic tophaceous gout of bilateral feet. **a, b** Axial bilateral forefeet (**a**) and corresponding dual-energy CT images (**b**) demonstrates extensive hyperdense lesions (arrows) surrounding the left 1st to 3rd metatarsophalangeal joints, some causing pressure erosions, that are composed of MSU crystals. Minimal MSU deposit is also seen in the right 2nd web space. **c** Three-dimensional (3D) reconstruction depicts multifocal MSU deposits scattered in bilateral feet, left more pronounced than right, and causing erosions more prominent around the left first and second metatarsophalangeal joints

crystals and establish a specific diagnosis [3] (Fig. 9). The gold standard to classify gout in the updated European League Against Rheumatism 2018 recommendations is through aspiration of joint or tophus to detect the presence of MSU crystal [33]. However, DECT is more useful than joint fluid aspiration in certain scenarios such as when MSU crystals are absent in joint fluid but aggregate around extra-articular sites [34]. DECT is a reliable alternative to detect MSU crystals when synovial fluid aspiration fails or is not feasible. On US, tophi are usually echogenic, heterogeneous, ill defined, multiple grouped, and surrounded by an anechoic halo. Associated findings such as bony erosions and "double contour" sign can also be identified [35, 36]. The sensitivity and specificity of US in the detection of gouty arthritis are 76.9% and 84.3% respectively [37]. In MRI, tophi typically show low T1 signal, intermediate to high T2 signal, and heterogeneous enhancement [38]. Multifocal lesions favor gout over neoplasm. Tophaceous gout can mimic a malignant soft tissue tumor [39]. When biopsy is considered in indeterminate cases, caution must be exercised in not placing the biopsy samples in formalin as the MSU crystals can dissolve in formalin and confound the diagnosis [18].

Fig. 10 A 37-year-old male with calcium hydroxyapatite deposition disease. He presents with chronic right shoulder pain. **a** Radiography shows rotator cuff calcifications contiguous with a cortical break and extending into the right humeral head. **b** Coronal CT confirms and better delineates these findings. **c** Coronal proton density-weighted fat suppression sequence shows extensive perilesional edema in the humeral head. The supraspinatus tendinous calcifications are poorly seen on MRI

Calcium hydroxyapatite deposition disease

Calcium hydroxyapatite deposition disease (HADD) is characterized by periarticular calcium hydroxyapatite depositions, most notably in the tendons and bursae. When crystals are shed intra-articularly, acute, often highly destructive arthropathy can develop (e.g., Milwaukee shoulder). Destructive arthropathy is more frequent in women between the ages of 50 and 90 and is bilateral in 65% of cases. Trauma or excessive use is noted in 25% of cases [40]. Most calcifications are asymptomatic and incidental findings. The deposits can resorb locally or extrude in adjacent bursa, joint, or bone. This extrusion can be chronic (asymptomatic or chronic pain) or acute and associated with severe pain [40]. The calcific deposit can be of varying size and does not correlate with the severity of symptoms [41]. Calcium HADD is often mono-articular and most commonly affects the shoulder, followed by the hip, knee, elbow, wrist, and hand [40].

Radiography is the primary imaging modality for diagnosis of calcium HADD. The calcification appears as amorphous, dense, well-defined, round, or oval-shaped deposits on radiograph and CT. When calcifications resorb, they tend to become cloudy, less dense, and poorly defined and can extend into adjacent structures: bursae, joints, or bone (Fig. 10). During acute resorption episodes, calcification may not be identified with radiographs [42]. On US, the calcium aggregates are echogenic with variable acoustic shadowing depending on the calcium aggregates' degree of consistency [43]. CT can depict tendinous calcifications and the extension of calcific deposits into adjacent tissues, including subcortical erosions and even penetration into adjacent bone [44, 45] (Fig. 10). DECT can help differentiate between calcium hydroxyapatite crystals and calcium pyrophosphate crystals with moderate accuracy by characterizing their DECT attenuation biochemical signatures [46]. MRI is not the modality of choice for the evaluation of HADD. In MRI, calcium hydroxyapatite deposits when seen appear as T1 and T2 hypointense areas [47]. However, the use of susceptibility-weighted imaging can reliably detect calcifications in the rotator cuff [48]. Surrounding soft tissue and joint inflammation as well as bone marrow edema are well visualized during the acute phases of HADD [44] (Fig. 10). Interpretation with MRI complemented with radiographs or CT can avoid misdiagnosis in rare cases of osseous involvement. In Milwaukee shoulder, the typical imaging findings are narrowing of the glenohumeral joint, destruction of subchondral bone and osteophytes, capsular and soft tissue calcification, and intra-articular loose bodies. In addition, MRI also shows rotator cuff tears and chondral thinning [49] (Fig. 11). When intra-articular, calcium hydroxyapatite crystals are too small to be reliably detected microscopically.

Calcium pyrophosphate deposition disease

Calcium pyrophosphate deposition disease (CPDD) arthropathy is characterized by the deposition of calcium pyrophosphate crystals in and around joints. Predisposing factors include age, genetics, osteoarthritis, and the use of loop diuretics [50]. CPPD is associated with other metabolic disorders such as hyperparathyroidism and hemochromatosis and has an unclear relationship with osteoarthritis [51]. It can present as acute

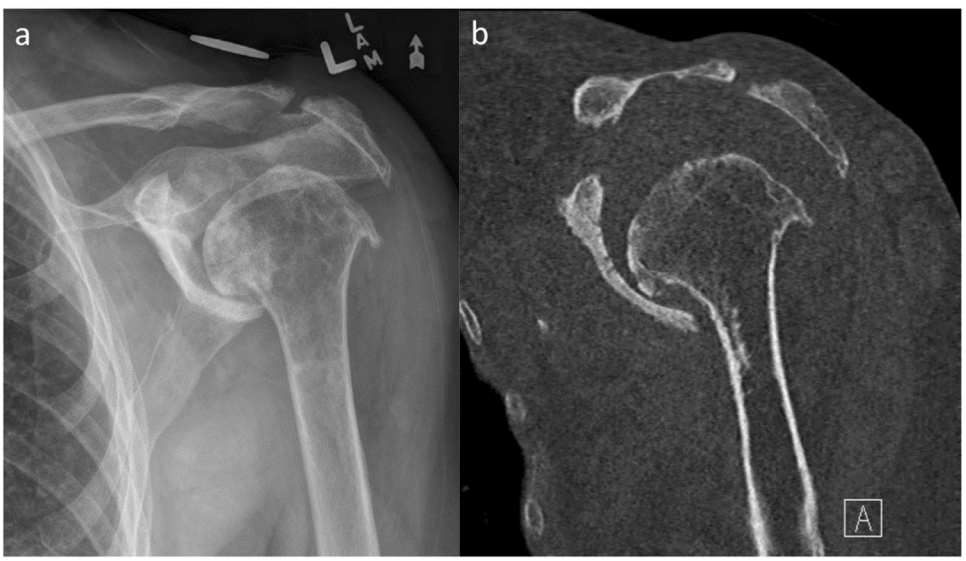

Fig. 11 A 81-year-old woman with Milwaukee shoulder. She presents with left shoulder swelling. **a, b** Left shoulder radiograph (**a**) and coronal CT left shoulder (**b**) show decreased glenohumeral joint space, bone sclerosis, destruction of subchondral bone and osteophytes, soft tissue calcification, and intra-articular loose bodies

Fig. 12 A 93-year-old man with calcium pyrophosphate deposition disease (CPPD). Left hand anteroposterior radiograph shows chondrocalcinosis projected over the radiocarpal joint, triangular fibrocartilage complex, and adjacent to the middle finger carpometacarpal joint with hook-like osteophytes of the middle finger metacarpal head and associated decreased joint spaces. Calcific densities are noted radial to the index finger distal interphalangeal joint and radial to the first carpometacarpal joint. Incidental background of osteopenia, old fractures of the distal radius and ulnar styloid, and degenerative changes of the thumb carpometacarpal joint

arthritis, chronic arthritis, or destructive arthropathy [40]. Common sites include the knee (especially the patellofemoral compartment), pubic symphysis, wrist (usually associated with scapholunate advanced collapse), and the spine. CPPD tends to be symmetrical in distribution and can manifest as chondrocalcinosis (mostly associated with CPPD), along with synovial, ligamentous/tendon, and soft tissue deposits of pyrophosphate. The absence of chondrocalcinosis in radiographs does not exclude the diagnosis of CPPD, especially during an acute flare [40]. A predilection for non–weight-bearing joints such as the elbow, metacarpophalangeal, and radiocarpal joints, a paucity/absence of osteophytes relative to the degree of joint space narrowing, and presence of calcific deposits can help differentiate CPPD from osteoarthritis [52] (Fig. 12). On CT, calcium pyrophosphate deposits appear denser than MSU deposits, with attenuation around 450 HU [52]. They tend to appear fine and linear in hyaline cartilage and articular capsule and show thicker frequently granular and stratified pattern in fibrocartilage, amorphous calcifications in synovial membranes and bursae, linear, and stratified in tendons and ligaments, as well as a pseudo-tumoral form mimicking sarcoma [40, 53]. DECT can be used for diagnosing CPPD by demonstrating the presence of calcium and absence of MSU crystals [54]. However, DECT cannot identify early non-calcified manifestations of CPPD [55]. The sensitivity of DECT in detecting CPDD is inferior to detection of gout but higher than that for radiographs. Specificity is similar to that of radiography [56]. MRI shows no additional role in evaluating CPDD, only demonstrating joint effusion and soft tissue inflammation during acute flares. Calcium pyrophosphate deposits show linear or punctate low-signal areas within articular or periarticular structures, with peripheral enhancement [57].

Tumor

Synovial sarcoma

Synovial sarcoma is the fourth most common soft tissue sarcoma and does not arise from synovium but from primitive mesenchymal cells that undergo differentiation to resemble synovial cells. Synovial sarcoma occurs with equal gender predisposition and in the adolescent and young adult demographics [58]. Synovial sarcomas manifest as slowly growing, sometimes painful, masses. Most tumors are larger than 5 cm, unless in the extreme periphery, likely due to earlier detection. This neoplasm is found mostly in the extremities around a joint, more commonly in the lower limbs. Calcification occurs in up to 30% of synovial sarcomas at radiography. Calcifications are variable in appearance but typically fine/sand-like and often eccentric or peripheral [58] (Fig. 13). Chondroid or osteoid lesional mineralization has been rarely described [59]. Larger masses may demonstrate the "triple sign" (low, intermediate, and high signal intensity to fat within the lesion attributed to fibrous tissue, calcium, hemorrhage, and/or necrosis) or the "bowl of

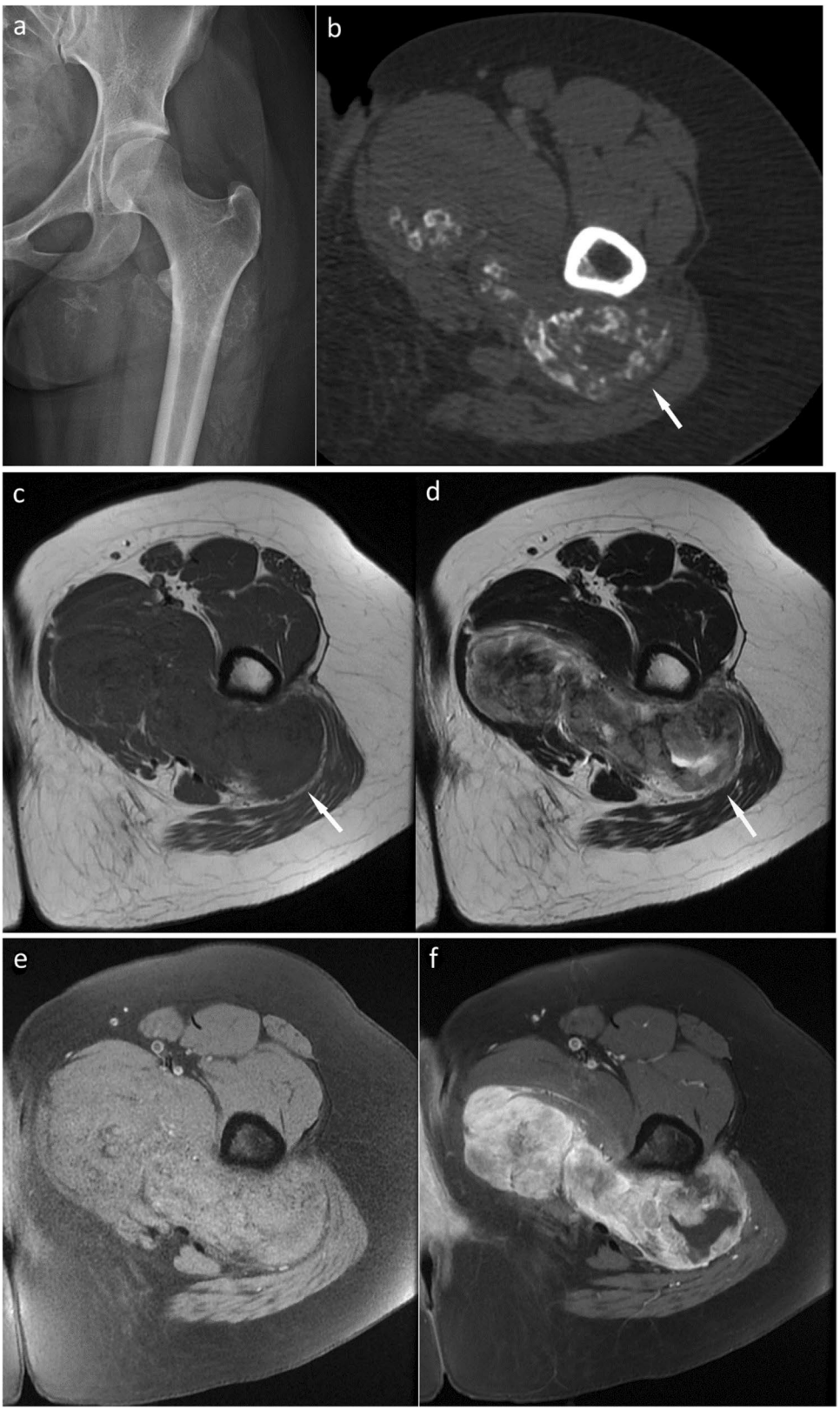

Fig. 13 A 23-year-old woman with synovial sarcoma. **a** Left hip radiograph shows extensive coarse and stippled calcifications projected over the left hip at the subtrochanteric region. **b** Axial CT shows an intermuscular mass displaying internal coarse and stippled calcifications forming conglomerates in the adductor compartment of the proximal thigh extending into the deep gluteal space. **c** Axial T1-weighted image shows this lesion (arrow) to be T1 isointense to muscle with internal T1 signal hypointense foci consistent with calcifications. **d** Axial T2-weighted image demonstrates the "triple" sign exhibited by the lesion (arrow). **e, f** pre- (**e**) and postgadolinium (**f**) T1-weighted image shows this mass to heterogeneously enhancing. The sciatic nerve is deviated medially but shows no signal abnormalities

grapes sign" (loculations and septations in the mass) [58] (Fig. 13). The classical appearance of smaller lesions is that of a homogeneous T1 hypointense, T2 hyperintense round circumscribed mass. Consequently, as they can be indolent, synovial sarcomas are frequently misdiagnosed as cysts. Similarly, on US, these lesions can appear round,

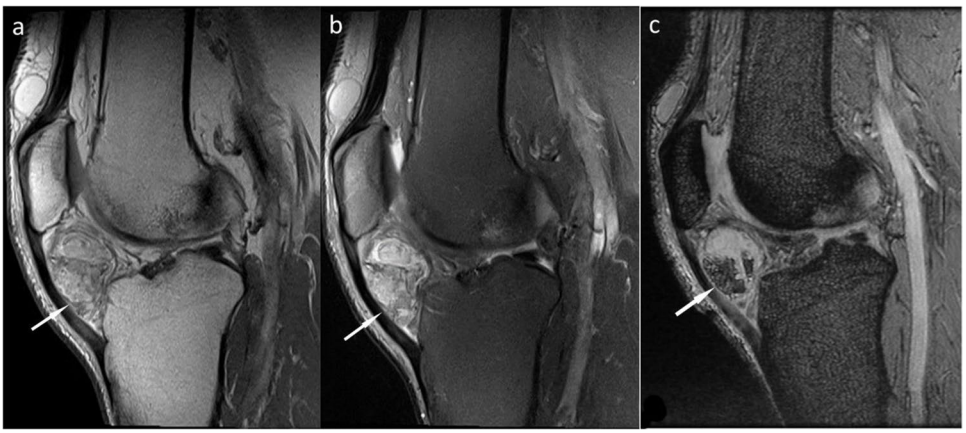

Fig. 14 A 62-year-old man with intracapsular chondroma. **a, b, c** Left knee sagittal T1-weighted image (**a**), sagittal proton density-weighted fat suppression image (**b**), and sagittal gradient echo (GRE) image (**c**) show a lobulated infrapatellar heterogeneous mass with internal T1 hyperintense foci that shows fat suppression and internal trabeculae compatible with ossification (arrow). This mass displaces the patellar tendon anteriorly

well circumscribed, and hypoechoic and may show posterior acoustic enhancement. When a cyst-like lesion has atypical features or location, intravenous contrast may assist in determining if it is solid. Up to 50% of synovial sarcomas show local recurrence within 2 years. However, these lesions may require longer follow-up since late local recurrences and metastasis of more than 5 years after initial diagnosis are common [60].

Synovial chondromatosis

Synovial chondromatosis can be classified into primary and secondary forms. Primary synovial chondromatosis is a benign synovial proliferative disorder in the joints, tendons, and bursae in which nodules detach from the synovium and undergo cartilaginous metaplasia with the formation of multiple intra-articular bodies. Secondary synovial chondromatosis is associated with joint derangements, such as mechanical or arthritic conditions, that cause intra-articular chondral bodies. The intra-articular bodies may calcify or ossify (Fig. 14).

Patients present with pain, decreased range of motion, or a locking/catching sensation. The knee, hip, elbow, and shoulder are most commonly affected. In the primary disease, radiographs show numerous intra-articular rounded, calcified/ossified bodies ranging from 1 to 20 mm relatively uniform in size and associated with an effusion, in contrast to the fewer number and more variably sized intra-articular fragments seen in the secondary form [8] (Figs. 15 and 16). Absence of any underlying joint abnormality features (most commonly, osteoarthritis) also helps differentiate primary synovial

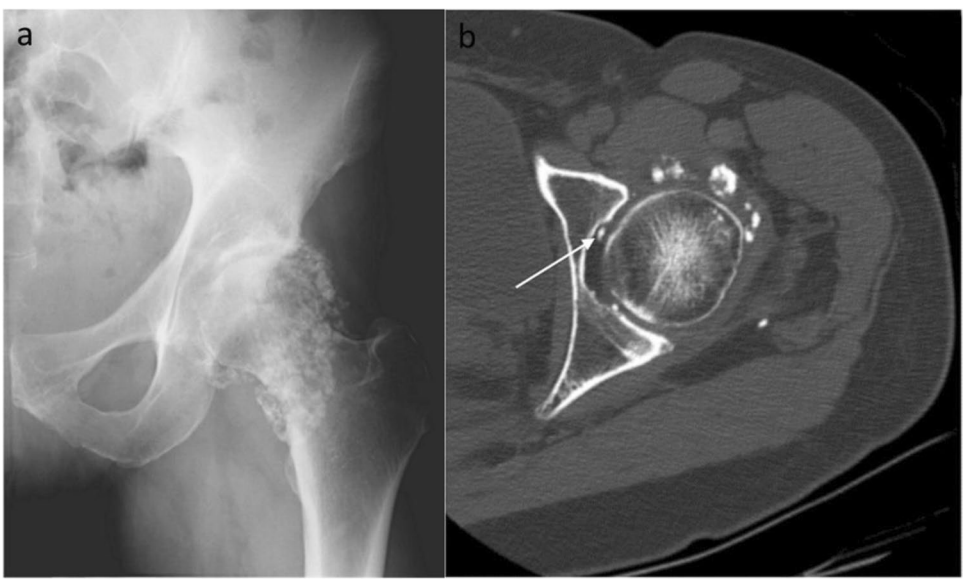

Fig. 15 A 54-year-old woman with primary synovial chondromatosis. **a** Left hip anteroposterior radiograph shows innumerable small ossific bodies of uniform size scattered within the confines of the left hip joint space. **b** Axial CT confirms these small intra-articular ossific bodies with one exerting extrinsic erosion of the left acetabulum (arrow) at the anterior margin of the cotyloid fossa

Fig. 16 A 36-year-old man with secondary synovial chondromatosis. Several ossific bodies of varying sizes scattered superior to the humeral head and over the axillary recess. The humeral head shows subchondral lucencies and an irregular contour suggestive of degenerative change

Fig. 17 A 41-year-old man with a broken sewing needle lodged in the right middle finger. **a, b** Right index finger anteroposterior radiograph (**a**) and lateral radiograph (**b**) shows a small linear metallic density structure with a tiny pinhole projected over the dorsal soft tissues of the index finger middle phalanx

chondromatosis from the secondary disease. These intra-articular nodules can show a typical chondroid ring-and-arc mineralization pattern or a target appearance when calcified, or a peripheral cortical rim with internal trabeculae when ossified [61]. These intra-articular bodies can cause pressure erosions of the adjacent bones and secondary osteoarthritis can develop. Radiographic findings of tenosynovial and bursal chondromatosis are similar to those of intra-articular disease, with calcification seen in approximately 60–100% of cases, and a mineralization identical to that of its intra-articular counterpart [62]. Other findings include clustering of mineralized bodies in the expected location a known bursa and round to oval or elongated mineralization confined within a tendon sheath. CT is useful for evaluating calcifications and detecting bony erosions. MRI show variable signal pattern dependent on the extent of calcification/ossification. Enhancement characteristic may resemble that of chondroid lesions with a characteristic peripheral and septal pattern [61]. The intra-articular bodies may extend into a Baker's cyst when arising in the knee and in the authors' experience uncommonly can be mistaken for synovial sarcoma. Primary synovial chondromatosis can rarely undergo malignant transformation to synovial chondrosarcoma [61].

Soft tissue chondroma

Soft tissue chondromas are benign extra-articular cartilaginous tumors sharing histological features with synovial chondromatosis [63]. These lesions occur over a wide age group and are slightly more common in males (3:2) [64]. Soft tissue chondromas occur most commonly in the hands and feet and are found near tendons and joints [64].

Soft tissue chondromas are lobulated with central and peripheral calcifications being arc like, punctate, spiculated, or coarsely geometric [65]. On MRI, soft tissue chondromas are T2 hyperintense but may show

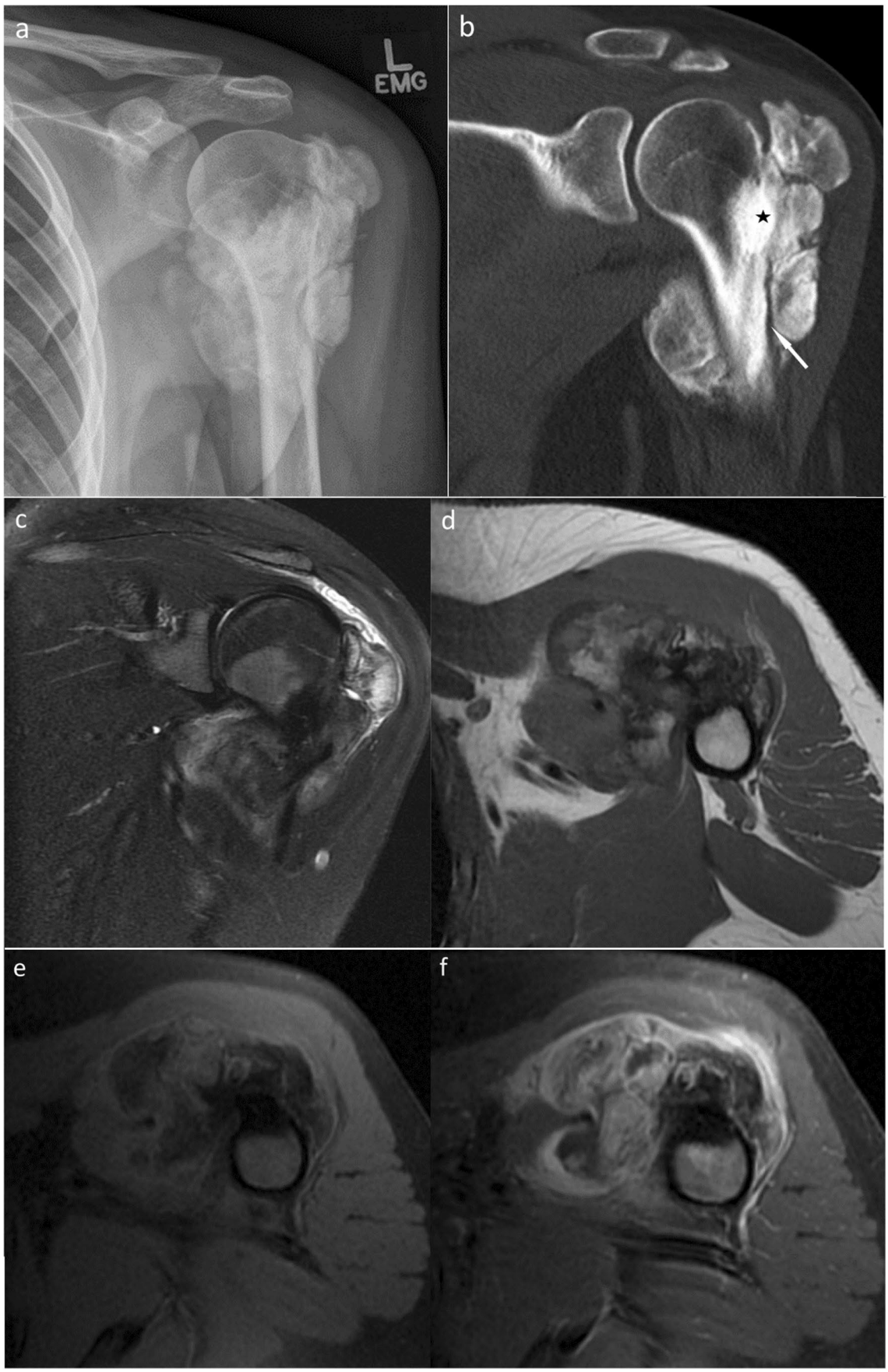
a
L
EMG
b
c
d
e
f

◂**Fig. 18** A 25-year-old woman with parosteal osteosarcoma. **a** Left shoulder anteroposterior radiograph shows a lobulated exophytic ossified mass arising from the proximal humerus metaphysis. **b** Coronal CT delineates the wide stalk of attachment (star) and radiolucent cleavage plane separating it from bone (arrow). **c, d, e, f** Coronal T2 fat suppression image (**c**), axial T1-weighted (**d**), pre- (**e**) and postgadolinum T1 fat suppression images (**f**) shows this lesion to have a heterogeneous appearance and heterogeneous enhancement

small internal signal hypointensities due to matrix calcifications [64].

Intracapsular chondroma, also known as intracapsular osteochondroma or soft tissue osteochondromatosis, is a rare benign lesion arising from extrasynovial metaplasia in the capsule or adjacent connective tissues [66]. Intracapsular chondroma is typically sited inferior to the patella in the region of the Hoffa fat pad. Some authors consider this entity as an end-stage form of Hoffa disease. On radiograph and CT, it appears as a calcified and/or ossified mass within the

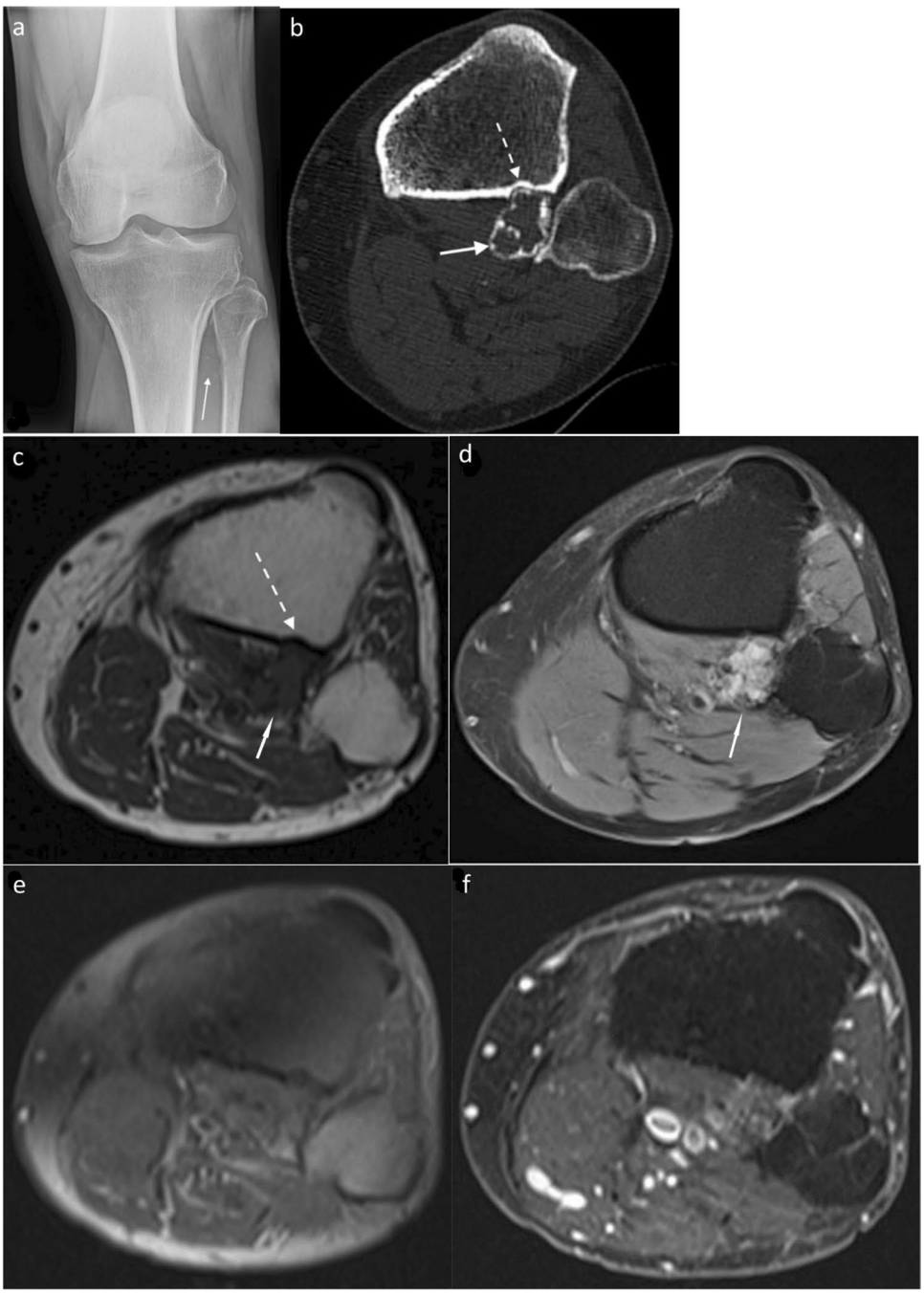

Fig. 19 A 73-year-old man with periosteal chondroma. **a** Left knee radiograph shows a subtle calcified lesion projected inferior the proximal tibiofibular joint (arrow) causing mild erosion of the proximal fibular shaft. **b** Axial CT shows this juxtacortical lobulated soft tissue lesion (solid arrow) with internal "ring and arc" calcifications scalloping the adjacent posterolateral tibial condyle (dashed arrow) and proximal fibular shaft. **c, d** Axial T1-weighted (**c**) and proton density (PD) weighted fat suppression (FS) images (**d**) shows this lesion (solid arrow) to be T1 isointense and PD FS hyperintense with peripheral and internal curvilinear signal hypointensities corresponding to calcifications. Adjacent pressure erosion of the posterolateral tibial condyle is noted (dashed arrow). **e, f** pre- (**e**) and postgadolinium T1-weighted FS (**f**) images shows mild peripheral enhancement of this lesion

infrapatellar fat pad and can produce bone erosion. MRI demonstrates a heterogeneous mass on T1- and T2-weighted sequences with high T2 signal intensity representing chondroid matrix or edema and areas of low T1/T2 signal intensity representing calcification or ossification [66] (Fig. 14).

Foreign body

Foreign body (FB) is an object lodged in the body usually from a penetrating injury. FB can be made of any material with the most common types being wood, glass, and metal [67]. Rarely, FB can arise from iatrogenic causes such as a retained fractured drainage catheter or present as a gossypiboma [68].

Although FBs may be asymptomatic, it can lead to complications such as infection, delayed wound healing, inflammation, and loss of function. The higher the atomic number and density of the FB, the greater the detectability by radiography. Radiographs are the first-line modality used to detect FBs [67, 69] (Fig. 17). FBs composed of metal, glass, stone, and calcified biologic such as sea urchin spines are radiopaque while those of wood and plastic are radiolucent [69]. The detectability of glass is dependent mainly on the size and density of the glass fragment, and glass FBs larger than 2 mm can be depicted at conventional radiography in almost all cases [67, 69, 70].

US can be used to detect radiographically occult foreign bodies (especially useful in the extremities and with wood), which invariably appears as hyperechoic and may or may not exhibit posterior acoustic shadowing or reverberation artifacts, depending on the material composition and angle of insonation [69]. If an FB is suspected but is occult on radiographs and US, CT is the next best modality for further evaluation [69]. CT allows precise localization of radiopaque FBs. Nonradiopaque FBs such as wood are moderately hyperattenuating on CT and can be detected but are best visualized when utilizing a wide window setting [67]. FBs comprising of glass have attenuation similar to that of calcium and bone (500 to HU) and those composed of calcified biologics have calcium attenuation that reduces with time as they undergo resorption [69]. MRI has suboptimal sensitivity and specificity in detecting foreign bodies but is superior to other imaging modalities in demonstrating complications and evaluating differential diagnoses [69]. FBs are signal hypointense on T1- and T2-weighted sequences.

Developmental

Accessory ossicles/sesamoids

Sesamoids are bony structures within a tendon and accessory ossicles derive from unfused accessory ossification centers. Although these structures are frequently

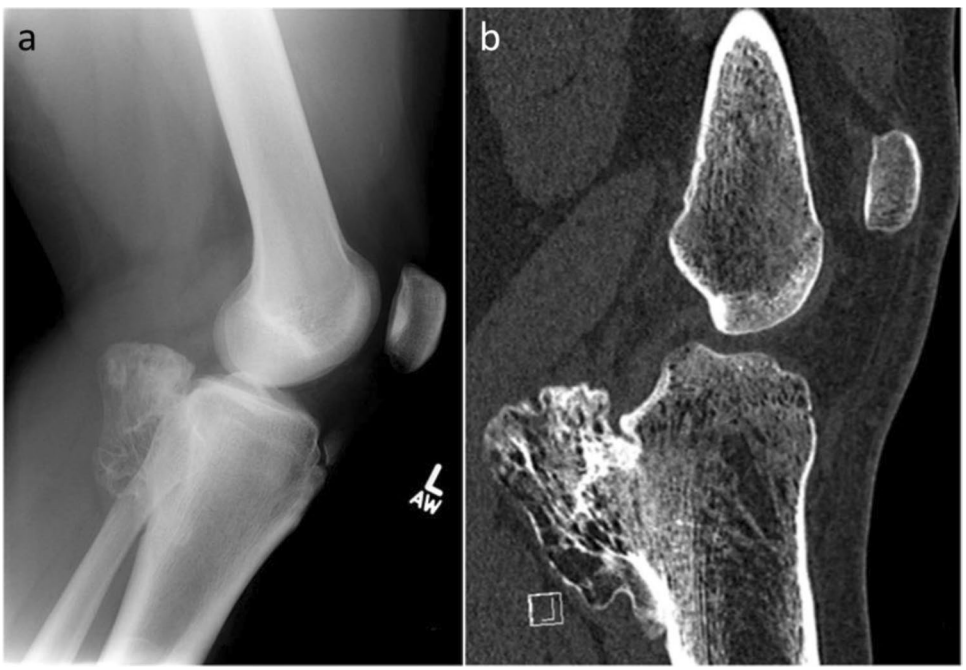

Fig. 20 A 24-year-old man with osteochondroma. **a, b** Left knee lateral radiograph (**a**) and sagittal CT (**b**) show a large bony spur exhibiting cortical and medullary continuation arising from the posterior knee metaphysis

Fig. 21 A 70-year-old man with psoriatic arthropathy and extensive ▶ psoriatic related bony proliferation and periostitis. Right index finger radiograph demonstrates marginal bone erosion with prominent irregular cortical thickening and bone proliferation (arrow) at the proximal interphalangeal joint. Minimal similar changes are seen in the distal interphalangeal joint

asymptomatic, they can cause degenerative changes, stress, and painful syndromes and undergo or simulate fractures [24]. Accessory ossicles and sesamoids occur at characteristic locations, are usually well corticated and regular in appearance, and can be multipartite [24]. Displacement of the accessory ossicles and sesamoids could indicate underlying tendinous or ligamentous injury respectively [24].

Mimickers

Trauma/stress

Enthesophyte

Enthesophytes are bony spurs that form at the attachment of a tendon, ligament, or joint capsule onto bone. Enthesophytes are oriented along traction forces and develop in response to repetitive mechanical stress or a more generalized inflammatory condition.

Bizarre parosteal osteochondromatous proliferation

Bizarre parosteal osteochondromatous proliferation (BPOP), otherwise known as Nora lesion, is a benign parosteal bony excrescence more common in young patients (20–30 years old) and is seen equally in males and females. BPOP is likely reactive, with a relationship to trauma suggested but not proved. BPOP usually occurs in the tubular bones of the hands and feet. On radiography, BPOP are located adjacent to the bony cortex but do not show intramedullary continuation. BPOP can grow rapidly and cause pain which can be mistaken for a more aggressive lesion.

Florid reactive periostitis

Florid reactive periostitis is an aggressive periosteal reaction of the hands and feet associated with an intact phalanx and a soft tissue swelling of benign etiology out of proportion to the periosteal reaction [71]. This lesion can mimic osteosarcoma and osteomyelitis. A combination of early follow-up radiograph within 7–10 days, and clinical assessment can distinguish it from osteomyelitis [71].

Tumor

Surface bone sarcomas/tumors

Surface bone sarcomas/tumors with a preference for metaphyseal location such as parosteal osteosarcoma and periosteal chondrosarcoma and chondroma can mimic calcified or ossified periarticular lesions. Parosteal osteosarcoma is the commonest subtype of surface osteosarcomas. Parosteal osteosarcoma is usually a lobulated, exophytic metaphyseal mass with soft tissue component showing central ossification (T2 high signal soft tissue mass with central low signal), shows a thin radiolucent cleavage plane separating it from bone, and has a wide or narrow "stalk" of attachment [72] (Fig. 18).

Periosteal chondroma

Periosteal chondroma is a benign chondral tumor originating from the periosteum with a predilection for the metaphyses of long tubular bones, hands and feet, and the bony insertions of tendons and ligaments [73]. Periosteal chondroma is characterized by a juxtacortical lobulated soft tissue lesion displaying a chondroid matrix. On radiography, the calcified chondroid matrix can be seen with saucerization of the adjacent cortex (Fig. 17). On MRI, periosteal chondroma can show high signal on T2-weighted sequences with peripheral and septal enhancement. Imaging features of periosteal chondroma and periosteal chondrosarcoma often show overlap [74]. A larger size exceeding 3 cm and a tendency to infiltrate into surrounding soft tissues can help differentiate periosteal chondrosarcoma from periosteal chondroma [74, 75] (Fig. 19).

Developmental

Osteochondroma

Osteochondroma is a developmental bone lesion composed of cortical and medullary bone with an overlying hyaline cartilage cap. Osteochondroma arises from metaphysis, grows away from the epiphysis, and demonstrates continuity with the bone marrow of the involved bone (Fig. 20). These lesions may be solitary or multiple and can cause complications related to mass effect, bursa formation, fracture, or malignant transformation.

Inflammatory arthropathy

Psoriatic-related bone proliferation and periostitis

Psoriatic-related bone proliferation is characterized by an irregular and indistinct marginal bone about the involved joint, causing a "fuzzy"/fluffy periostitis appearance or "whiskering" [76] (Fig. 21). Periostitis has a few configurations: It may appear as a thin periosteal layer of new bone adjacent to the cortex, a thick irregular layer, or irregular cortical thickening [76] (Fig. 21). Periostitis may develop in a region unaffected by bone erosions. Other features of inflammatory arthropathy aid in the diagnosis.

Iatrogenic

Metallosis

Metallosis is an uncommon complication resulting from infiltration of periprosthetic soft tissues and bone by metallic debris resulting from wear of joint arthroplasties. It is

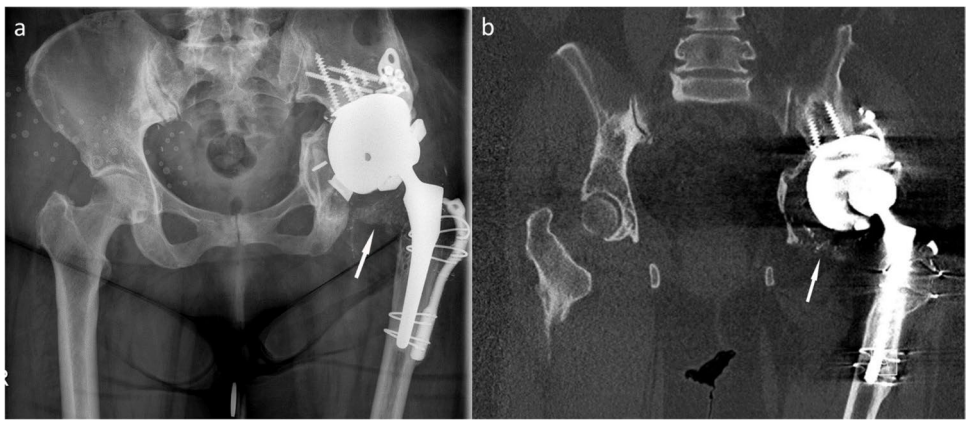

Fig. 22 A 70-year-old woman with metallosis. The patient is status post left acetabular plate and screw fixation and left total hip arthroplasty, with plate and screw fixation along the left proximal femur. **a, b** Pelvis radiograph (**a**) and coronal CT (**b**) show multiple metallic debris outlining the left inferomedial hip joint space. Additionally, there is a fractured screw in the left quadrilateral plate, protrusion acetabuli prosthetica, acetabulum osteolysis with loosening of the acetabular component and its consequent superolateral migration

usually associated with metal-on-metal arthroplasties but has been described in prostheses with non-metallic components [77]. On radiography, there can be eccentric alignment of the femoral component in the acetabular cup of a hip prosthesis in addition to the "bubble sign" (bubble-like hyperdensities outlining the joint space) and "cloud" sign (amorphous cloudy hyperdensities in the periprosthetic tissues) [78] (Fig. 22). In severe cases, metallosis may manifest as gross metallic particles in the periprosthetic tissues, which may eventuate in extensive surrounding osteolysis. CT better depicts the dense metal outlining the affected joint. MR imaging findings of metallosis include synovitis with signal hypointense debris that often demonstrates features of magnetic susceptibility and adjacent bony erosion [79]. Signal hypointense foci and susceptibility artifact within the pelvic lymph nodes may also be seen.

Conclusion

Periarticular mineralization is a common entity in the radiologist's daily reporting, encountered either incidentally or with respect to the clinical question. A systemic approach of distinguishing between calcification and ossification and classifying according to the different etiologies and presence of multifocality can narrow the differential list for the radiologist and aid in the diagnosis.

Abbreviations HU: Hounsfield unit; CT: Computed tomography; DECT: Dual-energy CT; MRI: Magnetic resonance imaging; US: Ultrasound; ISSVA: International Society for the Study of Vascular Anomalies; FDG: Fluorodeoxyglucose; PET: Positron emission tomography; MSU: Monosodium urate; HADD: Calcium hydroxyapatite deposition disease; CPDD: Calcium pyrophosphate deposition disease; FB: Foreign body; BPOP: Bizarre parosteal osteochondromatous proliferation; STIR: Short tau inversion recovery; 3D: Three-dimensional; GRE: Gradient echo; PD: Proton density; FS: Fat suppression

Declarations

Competing interests The authors declare no competing interests.

References

1. de Faria LL, Babler F, Ferreira LC, de Noronha Junior OA, Marsolla FL, Ferreira DL. Soft tissue calcifications: a pictorial essay. Radiol Bras. 2020;53:337–44.
2. Freire V, Moser TP, Lepage-Saucier M. Radiological identification and analysis of soft tissue musculoskeletal calcifications. Insights Imaging. 2018;9:477–92.
3. Mallinson PI, Coupal TM, McLaughlin PD, Nicolaou S, Munk PL, Ouellette HA. Dual-energy CT for the musculoskeletal system. Radiology. 2016;281:690–707.
4. Rajiah P, Sundaram M, Subhas N. Dual-energy CT in musculoskeletal imaging: what is the role beyond gout? Am J Roentgenol. 2019;213:493–505.
5. Adams LC, Bressem K, Böker SM, Bender Y-NY, Nörenberg D, Hamm B, Makowski MR. Diagnostic performance of susceptibility-weighted magnetic resonance imaging for the detection of calcifications: a systematic review and meta-analysis. Sci Rep. 2017;7:15506.
6. Hughes M, Hodgson R, Harris J, Porter N, Jackson S, Kirwadi A, Manning J, Peytrignet S, Herrick AL. Imaging calcinosis in patients with systemic sclerosis by radiography, computerised tomography and magnetic resonance imaging. Semin Arthritis Rheum. 2019;49:279–82.
7. Olsen KM, Chew FS. Tumoral calcinosis: pearls, polemics, and alternative possibilities. Radiographics. 2006;26:871–85.
8. Banks KP, Bui-Mansfield LT, Chew FS, Collinson F. A compartmental approach to the radiographic evaluation of soft-tissue calcifications. Semin Roentgenol. 2005;40:391–407.
9. Eisenberg B, Tzamaloukas AH, Hartshorne MF, Listrom MB, Arrington ER, Sherrard DJ. Periarticular tumoral calcinosis and hypercalcemia in a hemodialysis patient without hyperparathyroidism: a case report. J Nucl Med. 1990;31:1099.
10. Balin SJ, Wetter DA, Andersen LK, Davis MDP. Calcinosis cutis occurring in association with autoimmune connective tissue disease: the Mayo Clinic experience with 78 patients, 1996–2009. Arch Dermatol. 2012;148:455–62.
11. de Vuyst D, Vanhoenacker F, Gielen J, Bernaerts A, de Schepper AM. Imaging features of musculoskeletal tuberculosis. Eur Radiol. 2003;13:1809–19.
12. Lanzer P. Primary media sclerosis Mönckeberg: diagnostic criteria. Cor Vasa. 2018;60:e205–8.
13. ISSVA Classification of Vascular Anomalies ©2018 International Society for the Study of Vascular Anomalies Available at "issva.org/classification" Accessed 8 June 2021.
14. Flors L, Leiva-Salinas C, Maged IM, et al. MR imaging of soft-tissue vascular malformations: diagnosis, classification, and therapy follow-up. Radiographics. 2011;31:1321–40.
15. Flores D, v., Gómez CM, Estrada-Castrillón M, Smitaman E, Pathria MN, . MR imaging of muscle trauma: anatomy, biomechanics, pathophysiology, and imaging appearance. Radiographics. 2018;38:124–48.
16. Meyers C, Lisiecki J, Miller S, Levin A, Fayad L, Ding C, Sono T, McCarthy E, Levi B, James AW (2019) Heterotopic ossification: a comprehensive review. JBMR Plus 3:e10172
17. Walczak BE, Johnson CN, Howe BM. Myositis ossificans. J Am Acad Orthop Surg. 2015;23:612–22.
18. Kwee RM, Kwee TC. Calcified or ossified benign soft tissue lesions that may simulate malignancy. Skeletal Radiol. 2019;48:1875–90.
19. Shirkhoda A, Armin A-R, Bis KG, Makris J, Irwin RB, Shetty AN. MR imaging of myositis ossificans: variable patterns at different stages. J Magn Reson Imaging. 1995;5:287–92.
20. Zubler V, Mühlemann M, Sutter R, Götschi T, Müller DA, Dietrich TJ, Pfirrmann CW. Diagnostic utility of perilesional muscle edema in myositis ossificans. Skeletal Radiol. 2020;49:929–36.
21. Schulte M, Brecht-Krauss D, Heymer B, Guhlmann A, Hartwig E, Sarkar MR, Diederichs CG, Schultheiß M, Kotzerke J, Reske SN. Fluorodeoxyglucose positron emission tomography of soft tissue tumours: is a non-invasive determination of biological activity possible? Eur J Nucl Med. 1999;26:599–605.
22. Martin DA, Senanayake S. Myositis ossificans. N Engl J Med. 2011;364:758–758.
23. O'Dwyer HM, Al-Nakshabandi NA, Al-Muzahmi K, Ryan A, O'Connell JX, Munk PL. Calcific myonecrosis: keys to recognition and management. Am J Roentgenol. 2006;187:227.

24. Guo S, Yan YY, Lee SSY, Tan TJ. Accessory ossicles of the foot—an imaging conundrum. Emerg Radiol. 2019;26:465–78.
25. Narayanasamy S, Krishna S, Sathiadoss P, Althobaity W, Koujok K, Sheikh AM. Radiographic review of avulsion fractures. Radiographics. 2018;38:1496–7.
26. Tsionos I, Leclercq C, Rochet JM. Heterotopic ossification of the elbow in patients with burns. Results after early excision. Journal of Bone and Joint Surgery - Series B. 2004;86:396–403.
27. Orchard GR, Paratz JD, Blot S, Roberts JA. Risk factors in hospitalized patients with burn injuries for developing heterotopic ossification—a retrospective analysis. J Burn Care Res. 2015;36:465–70.
28. Kornhaber R, Foster N, Edgar D, Visentin D, Ofir E, Haik J, Harats M. The development and impact of heterotopic ossification in burns: a review of four decades of research. Scars, Burns & Healing. 2017;3:205951311769565.
29. Roddy E, Choi HK. Epidemiology of gout. Rheumatic Disease Clinics of North America. 2014;40:155–75.
30. Girish G, Melville DM, Kaeley GS, Brandon CJ, Goyal JR, Jacobson JA, Jamadar DA. Imaging Appearances in Gout. Arthritis. 2013;2013:1–10.
31. Abdellatif W, Ding J, Khorshed D, Shojania K, Nicolaou S. Unravelling the mysteries of gout by multimodality imaging. Semin Arthritis Rheum. 2020;50:S17–23.
32. Gerster JC, Landry M, Dufresne L, Meuwly JY. Imaging of tophaceous gout: computed tomography provides specific images compared with magnetic resonance imaging and ultrasonography. Ann Rheum Dis. 2002;61:52–4.
33. Richette P, Doherty M, Pascual E, et al. 2018 updated European League against Rheumatism evidence-based recommendations for the diagnosis of gout. Ann Rheum Dis. 2020;79:31–8.
34. Bongartz T, Glazebrook KN, Kavros SJ, et al. Dual-energy CT for the diagnosis of gout: an accuracy and diagnostic yield study. Ann Rheum Dis. 2015;74:1072–7.
35. Terslev L, Gutierrez M, Christensen R, et al. Assessing elementary lesions in gout by ultrasound: results of an OMERACT patient-based agreement and reliability exercise. J Rheumatol. 2015;42:2149–54.
36. Howard RG, Pillinger MH, Gyftopoulos S, Thiele RG, Swearingen CJ, Samuels J. Reproducibility of musculoskeletal ultrasound for determining monosodium urate deposition: concordance between readers. Arthritis Care Res. 2011;63:1456–62.
37. Ogdie A, Taylor WJ, Neogi T, et al. Performance of ultrasound in the diagnosis of gout in a multicenter study: comparison with monosodium urate monohydrate crystal analysis as the gold standard. Arthritis and Rheumatology. 2017;69:429–38.
38. Chen CKH, Yeh LR, Pan H, ben, Yang CF, Lu YC, Wang JS, Resnick D, . Intra-articular gouty tophi of the knee: CT and MR imaging in 12 patients. Skeletal Radiol. 1999;28:75–80.
39. Forbess LJ, Fields TR. The broad spectrum of urate crystal deposition: unusual presentations of gouty tophi. Semin Arthritis Rheum. 2012;42:146–54.
40. Jacques T, Michelin P, Badr S, Nasuto M, Lefebvre G, Larkman N, Cotten A. Conventional radiology in crystal arthritis: gout, calcium pyrophosphate deposition, and basic calcium phosphate crystals. Radiol Clin North Am. 2017;55:967–84.
41. Vinson EN, Desai S, v, Reddy S, Goldner RD, . AJR teaching file: periarticular calcifications in two patients with acute hand pain. Am J Roentgenol. 2010;195:S76–9.
42. Kraemer EJ, El-Khoury GY. Atypical calcific tendinitis with cortical erosions. Skeletal Radiol. 2000;29:690–6.
43. Farin PU. Consistency of rotator-cuff calcifications: observations on plain radiography, sonography, computed tomography, and at needle treatment. Invest Radiol. 1996;31:300–4.
44. Flemming DJ, Murphey MD, Shekitka KM, Temple HT, Jelinek JJ, Kransdorf MJ. Osseous involvement in calcific tendinitis: a retrospective review of 50 cases. Am J Roentgenol. 2003;181:965–72.
45. Marinetti A, Sessa M, Falzone A, della Sala SW, . Intraosseous migration of tendinous calcifications: two case reports. Skeletal Radiol. 2018;47:131–6.
46. Pascart T, Falgayrac G, Norberciak L, Lalanne C, Legrand J, Houvenagel E, Ea H-K, Becce F, Budzik J-F (2020) Dual-energy computed-tomography-based discrimination between basic calcium phosphate and calcium pyrophosphate crystal deposition in vivo. Therapeutic Advances in Musculoskeletal Disease 12:1759720X20936060
47. Zubler C, Mengiardi B, Schmid MR, Hodler J, Jost B, Pfirrmann CWA. MR arthrography in calcific tendinitis of the shoulder: diagnostic performance and pitfalls. Eur Radiol. 2007;17:1603–10.
48. Nörenberg D, Ebersberger HU, Walter T, Ockert B, Knobloch G, Diederichs G, Hamm B, Makowski MR. Diagnosis of calcific tendonitis of the rotator cuff by using susceptibility-weighted MR imaging. Radiology. 2015;278:475–84.
49. Jeong W, Kim J, Choi S, Kang H. Very rapidly progressive shoulder arthropathy with complete destruction of the humeral head. Journal of Rheumatic Diseases. 2019;26:142.
50. Abhishek A. Calcium pyrophosphate deposition disease: a review of epidemiologic findings. Curr Opin Rheumatol. 2016;28:133–9.
51. Zhang W, Doherty M, Bardin T, et al. European league against rheumatism recommendations for calcium pyrophosphate deposition. Part I: terminology and diagnosis. Ann Rheum Dis. 2011;70:563–70.
52. Buckens CF, Terra MP, Maas M. Computed tomography and MR imaging in crystalline-induced arthropathies. Radiol Clin North Am. 2017;55:1023–34.
53. Dharas M, Balogh P, Calleja M, Saifuddin A. Test yourself: a 49-year-old lady with a history of chronic left hip pain following a fall twenty months earlier. Skeletal Radiol. 2020;49:1495–6.
54. Kim HR, Lee JH, Kim NR, Lee SH. Detection of calcium pyrophosphate dihydrate crystal deposition disease by dual-energy computed tomography. Korean J Intern Med. 2014;29:404–5.
55. Budzik J-F, Marzin C, Legrand J, Norberciak L, Becce F, Pascart T. Can dual-energy computed tomography be used to identify early calcium crystal deposition in the knees of patients with calcium pyrophosphate deposition? Arthritis & Rheumatology. 2021;73:687–92.
56. Tanikawa H, Ogawa R, Okuma K, Harato K, Niki Y, Kobayashi S, Nagura T. Detection of calcium pyrophosphate dihydrate crystals in knee meniscus by dual-energy computed tomography. J Orthop Surg Res. 2018;13:73.
57. Beltran J, Marty-Delfaut E, Bencardino J, Rosenberg ZS, Steiner G, Aparisi F, Padrón M. Chondrocalcinosis of the hyaline cartilage of the knee: MRI manifestations. Skeletal Radiol. 1998;27:369–74.
58. Murphey MD, Gibson MS, Jennings BT, Crespo-Rodríguez AM, Fanburg-Smith J, Gajewski DA. From the archives of the AFIP: imaging of synovial sarcoma with radiologic-pathologic correlation. Radiographics. 2006;26:1543–65.
59. Sánchez Reyes JM, Alcaraz Mexia M, Quiñones Tapia D, Aramburu JA. Extensively calcified synovial sarcoma. Skeletal Radiol. 1997;26:671–3.
60. Krieg AH, Hefti F, Speth BM, et al. Synovial sarcomas usually metastasize after >5 years: a multicenter retrospective analysis with minimum follow-up of 10 years for survivors. Ann Oncol. 2011;22:458–67.
61. Murphey MD, Vidal JA, Fanburg-Smith JC, Gajewski DA. From the archives of the AFIP: imaging of synovial chondromatosis with radiologic-pathologic correlation. Radiographics. 2007;27:1465–88.
62. Fetsch JF, Vinh TN, Remotti F, Walker EA, Murphey MD, Sweet DE. Tenosynovial (extraarticular) chondromatosis: an analysis of

37 cases of an underrecognized clinicopathologic entity with a strong predilection for the hands and feet and a high local recurrence rate. Am J Surg Pathol. 2003;27:1260–8.
63. Amary F, Perez-Casanova L, Ye H, et al. Synovial chondromatosis and soft tissue chondroma: extraosseous cartilaginous tumor defined by FN1 gene rearrangement. Mod Pathol. 2019;32:1762–71.
64. Bancroft LW, Peterson JJ, Kransdorf MJ. Imaging of soft tissue lesions of the foot and ankle. Radiol Clin North Am. 2008;46:1093–103.
65. Hondar Wu HT, Chen W, Lee O, Chang CY. Imaging and pathological correlation of soft-tissue chondroma: a serial five-case study and literature review. Clin Imaging. 2006;30:32–6.
66. Jacobson JA, Lenchik L, Ruhoy MK, Schweitzer ME, Resnick D. MR Imaging of the Infrapatellar Fat Pad of Hoffa. Radiographics. 1997;17:675–91.
67. Jarraya M, Hayashi D, de Villiers R, v, Roemer FW, Murakami AM, Cossi A, Guermazi A, . Multimodality imaging of foreign bodies of the musculoskeletal system. Am J Roentgenol. 2014;203:W92–102.
68. Puvanesarajah V, Fayad LM, Rao SS, McCarthy EF, Morris CD. Extremity gossypiboma mimicking sarcoma: case report and review. Skeletal Radiol. 2019;48:629–35.
69. Carneiro BC, Cruz IAN, Chemin RN, Rizzetto TA, Guimarães JB, Silva FD, Yoshida Junior C, Pastore D, Ormond Filho AG, Nico MAC. Multimodality imaging of foreign bodies: new insights into old challenges. Radiographics. 2020;40:1965–86.
70. Horton LK, Jacobson JA, Powell A, Fessell DP, Hayes CW. Sonography and radiography of soft-tissue foreign bodies. Am J Roentgenol. 2001;176:1155–9.
71. Sundaram M, Wang L, Rotman M, Howard R, Saboeiro AP. Florid reactive periostitis and bizarre parosteal osteochondromatous proliferation: pre-biopsy imaging evolution, treatment and outcome. Skeletal Radiol. 2001;30:192–8.
72. Harper K, Sathiadoss P, Saifuddin A, Sheikh A. A review of imaging of surface sarcomas of bone. Skeletal Radiol. 2021;50:9–28.
73. Woertler K, Blasius S, Brinkschmidt C, Hillmann A, Link TM, Heindel W. Periosteal chondroma: MR characteristics. J Comput Assist Tomogr. 2001;25:425–30.
74. Robinson P, White LM, Sundaram M, Kandel R, Wunder J, McDonald DJ, Janney C, Bell RS. Periosteal chondroid tumors: radiologic evaluation with pathologic correlation. Am J Roentgenol. 2001;177:1183–8.
75. Chaabane S, Bouaziz MC, Drissi C, Abid L, Ladeb MF. Periosteal chondrosarcoma. Am J Roentgenol. 2009;192:W1–6.
76. Jacobson JA, Girish G, Jiang Y, Resnick D. Radiographic evaluation of arthritis: inflammatory conditions. Radiology. 2008;248:378–89.
77. Murali R, Bonar SF, Kirsh G, Walter WK, Walter WL. Osteolysis in third-generation alumina ceramic-on-ceramic hip bearings with severe impingement and titanium metallosis. J Arthroplasty. 2008;23:1240.e13-1240.e19.
78. Heffernan EJ, Alkubaidan FO, Nielsen TO, Munk PL. The imaging appearances of metallosis. Skeletal Radiol. 2008;37:59–62.
79. Fritz J, Lurie B, Miller TT, Potter HG. MR imaging of hip arthroplasty implants. Radiographics. 2014;34:E106–32.